

# Light scattering behavior to metasurfaces by diffusion model

Hay Lahav

ID: 308279918

Email: haylahav1@gmail.com

Nadav Marciano

ID: 305165698

Email: nadavmarci@gmail.com

October 2, 2023

## Abstract

In this project, we tackle the problem of creating a deep learning generative diffusion model capable of discerning and generating optimal meta-surface configurations based on the observed light-scattering behaviors. The training of our model relies on a dataset that encompasses metasurface samples and their corresponding light-scattering behaviors. Our approach to solving this problem is to use a *class-conditioned diffusion model* [1] based on 2dUnet from Hugging Face and adjust it according to our data. In addition, we had to adjust and improve the model architecture in order to optimize its performance. As part of our course project, we have obtained a diverse dataset containing 25000 meta surface patterns and their corresponding light scattering to advance our research. Following model training and testing, we successfully obtained the predicted metasurface configuration corresponding to a given matrix of light properties.

## 1. Introduction

This project embarks on the challenge of harnessing the potential of diffusion models to navigate the complex landscape of meta-surface design. Our goal is to fit each light properties matrix into a suitable metasurface pattern by diffusion model. In the present era, metasurfaces offer precise manipulation of light properties like phase, amplitude, and wavefront [2]. The objective, when provided with a dataset comprising metasurfaces and their interactions with light, is to train a diffusion model capable of identifying the most suitable meta-surface for a given measurement of light. A diffusion model is a parametrized Markov chain trained using variational inference techniques in order to generate samples that closely resemble the original data within a finite timeframe [3]. In essence, transitions of this chain are learned to reverse a diffusion process, which is a Markov chain that gradually adds noise to the data in the opposite direction of sampling, ultimately obscuring an underlying signal.

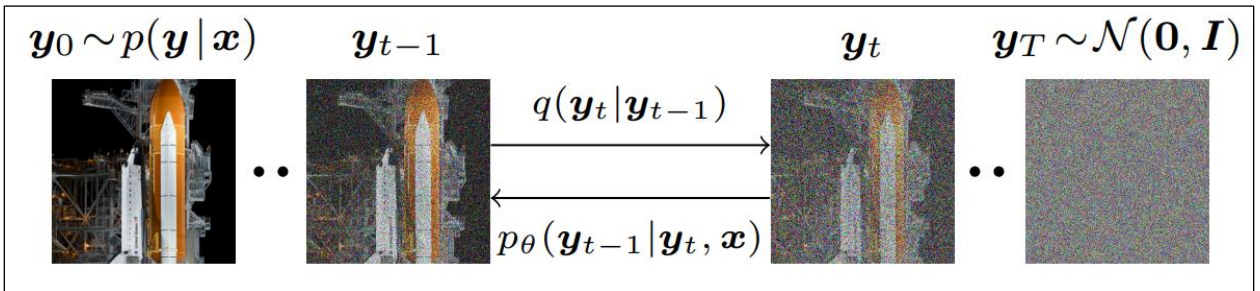


Figure 1: The directed graphical model [3].

This subject is important because diffusion models can be used in learning useful feature representations for scientific measurements and to generate a suitable output according to those measurements and the user demands. This area of study holds significant allure due to the versatile applications of diffusion models. They can serve various purposes, including generating images based on prompts or acquiring valuable feature representations. By adjusting the DDPM [5] to conditional image generation and using the Unet architecture from Hugging Face, we obtained after 50 epochs of training a satisfying prediction of the desired metasurface pattern given the data of the light matrices and their corresponding metasurface pattern.

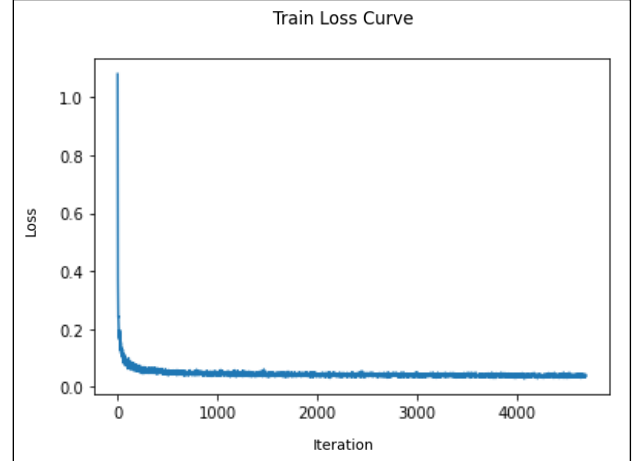


Figure 2: The training loss graph (batch =20, lr= 4e-3, MSELoss)

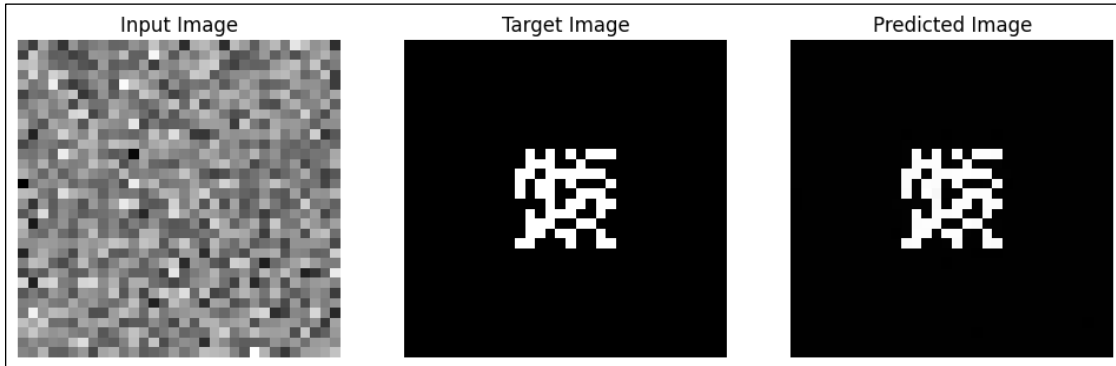


Figure 3: The model prediction in comparison to the required pattern based on the dataset.

The table shows that our model achieved 98.60% accuracy, 0.995 precision, and 0.995 recall. These results are relatively good, but we believe that there is room for improvement in the future.

## 2. Related Work

There are no existing implementations for our exact project, namely, fitting a meta-surface pattern in accordance with their corresponding light-scattering behaviors using diffusion models. We had to develop a custom solution for this specific classifying problem. Our search of relevant papers revealed that diffusion models are commonly used for segmentation and text-to-image generation tasks, such as Stable Diffusion model [4]. However, we did not find any diffusion model papers or projects that use light properties and patterns for image-to-image fitting tasks. On the other hand, we found classification papers that use the Generative Adversarial Network (GAN) model. The Unit architecture and the noise scheduler for the diffusion model were taken from the Diffusers library of Hugging Face [1]. In the Hugging Face website, there is an example of how to regenerate the

Type	Count
Correct Predictions	1972
Incorrect Predictions	28
Overall Image-Level Accuracy	98.60%
Average Precision for Individual Images	0.995
Average Recall for Individual Images	0.995

Table 1: Test results precision and recall

same images from the input data, meaning, the noised input images are represented in the output images. Vice versa to our project which has the goal to generate a correspondent pattern while the noised image represents the light properties.

### 3. Data

The data we are working with is light scattering from silicon surfaces. The material being studied is silicone, and the wavelength used is 1550nm. Prof. Scheuer's nano photonics lab at Tel Aviv University provided the dataset, containing twenty-five thousand samples. Each sample includes the following data:

- xx\_data: The material template is represented as a binary vector with a size of 100, arranged in a 10 x 10 matrix.
- h: The height of the template, which varies for each sample.
- Rm and Tm: Matrices representing the transmission and reflection of light, with vector lengths of 529, arranged in a 23 x 23 matrix.

The data was initially received in the form of MATLAB files. We loaded this dataset and converted it into a DataFrame, ensuring that each column contained the following information for each sample: xx\_data, h, Rm, and Tm. To match the UNET model architecture, we created two 32 x 32 matrices for each sample.

The pattern matrix is a binary matrix with one channel and padded the matrices with zeros to achieve a consistent 32 x 32 size:

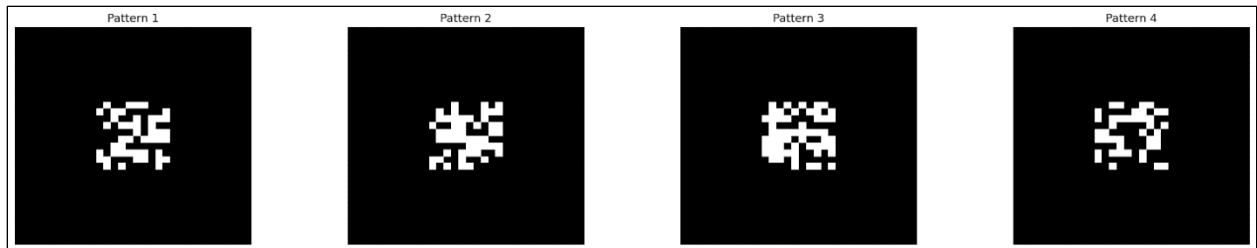


**Figure 4:** An example of the metasurface patterns of the first four samples.

The light matrix is a matrix with three channels:

Channel 1: Rm Matrix.

Channel 2: Tm matrix.

Channel 3: The height of the pattern multiplied by the binary pattern of the sample. we normalized and padded the matrices with zeros to achieve a consistent size of 32 x 32 and merged them together to form an “image”.

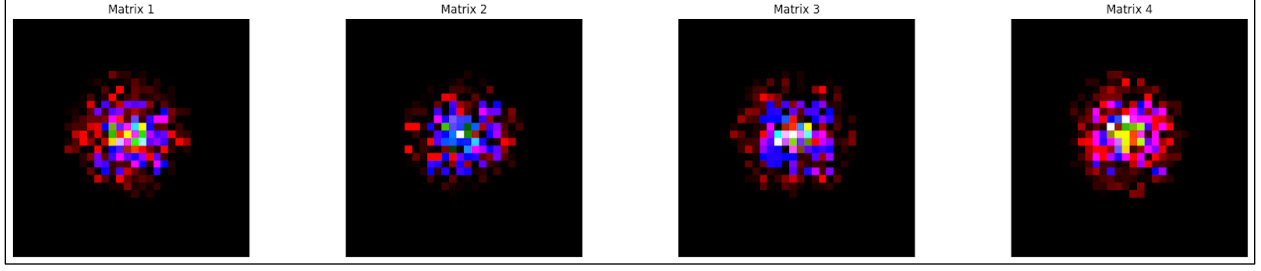


**Figure 5:** An example of the light matrices after normalization and padding of the first four sample.

We stored the data for each sample in a DataFrame, ensuring that each column contained the following information: the light matrix and `xx_data` (the pattern matrix). For further analysis, these matrices for each sample were transformed into tensors, and the dataset was divided into a training set consisting of 23 thousand samples and a test set consisting of 2 thousand samples.

## 4. Method

Diffusion models are a type of latent variable model, denoted as  $p_\theta(y_0)$ , defined through the integral of  $p_\theta(y_{0:T})$  over  $y_1, \dots, y_T$ , the latent variables of the same dimensionality as the data  $y_0 \sim p(y_0)$ . What sets diffusion models apart from other latent variable models is that the approximate posterior  $p(y_{1:T}|y_0)$ , known as the '**forward process**' is constrained to a Markov chain that gradually introduces Gaussian noise to the data following a predefined variance schedule  $\beta_1, \dots, \beta_T$ :

$$q(y_T|y_0) \equiv \prod_{t=1}^T q(y_t|y_{t-1}), \quad (1)$$

Where:

$$q(y_t|y_{t-1}) \equiv N(y_t; \sqrt{1 - \beta_t}y_{t-1}, \beta_t I).$$

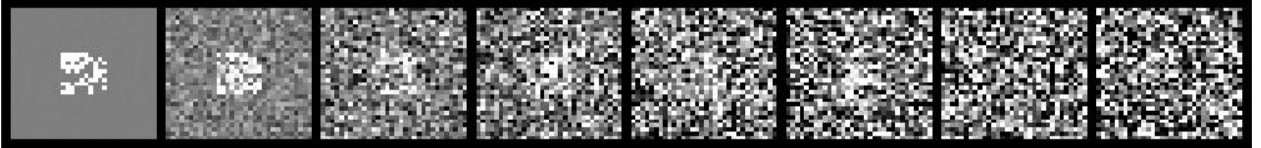


**Figure 6:** The forward diffusion process  $q$  (left to right) gradually adds Gaussian noise to the target image.

The joint distribution  $p(y_{0:T})$  is referred to as the '**reverse process**' and is defined as a Markov chain with learned Gaussian transitions, starting with  $p(y_t) = N(y_T; 0, I)$ . In other words, Inference in our model involves a reverse process that operates in the opposite direction of the initial diffusion process. This reverse process starts from a Gaussian noise  $y_T$  and aims to recover the original noise-free image  $y_0$ .

$$p(y_{0:T}) \equiv p(y_T) \prod_{t=1}^T p_\theta(y_{t-1}|y_t), \quad (2)$$

Where:

$$p_\theta(y_{t-1}|y_t) \equiv N(y_t; \mu_\theta(y_t, t), \Sigma_\theta(y_t, t))$$

and

$$p_\theta(y_{t-1}|y_t, x_0) = \mathcal{N}(y_{t-1}; \tilde{\mu}_t(x_t, x_0), \tilde{\tau}_t I).$$

#### 4.1 Optimizing

The training process involves optimizing the standard variational bound on the negative log likelihood:

$$E[-\log p_\theta(y_0)] \leq E_q \left[ -\log \left( \frac{p_\theta(y_{0:T})}{q(y_{1:T}|y_0)} \right) \right] = E_q \left[ -\log p(y_T) - \sum_{t \geq 1} \log \left( \frac{p_\theta(y_{t-1}|y_t)}{q(y_{t-1}|y_t)} \right) \right] = L \quad (3)$$

The forward process variances  $\beta_t$  can be either learned through reparameterization or set as hyperparameters. The expressive power of the reverse process is ensured, in part, by the choice of Gaussian conditionals in  $p_\theta(y_{t-1}|y_t)$ , especially when  $\beta_t$  values are small. A notable feature of the forward process is that it allows for the closed-form sampling of  $y_t$  at any timestep  $t$ , as equation (1) can be expressed by the following expression:

$$q(y_t|y_0) = \mathcal{N}(y_t; \sqrt{\bar{\alpha}_t}y_0 + (1 - \bar{\alpha}_t)I) \quad (4)$$

Where:

$$\alpha_t \equiv 1 - \beta_t \quad \text{and} \quad \bar{\alpha}_t \equiv \prod_{s=1}^t \alpha_s \quad \tilde{y} = \sqrt{\bar{\alpha}_t}y_0, (1 - \bar{\alpha}_t)$$

Efficient training is achievable by optimizing random terms of  $L$  (3) using stochastic gradient descent. Further enhancements can be made by rewriting the negative log likelihood  $L$  in a form that leverages the Kullback-Leibler (KL) divergence:

$$\mathbb{E}_k \left[ D_{KL}(q(y_T|y_0)||p(y_T)) \right] + \sum_{t \geq 1} D_{KL}(q(y_{t-1}|y_t, y_0)||p_\theta(y_{t-1}|y_t)) - \log p_\theta(y_0|y_1) \quad (5)$$

In Equation, KL divergence is used to directly compare  $p_\theta(y_{t-1}|y_t)$  against forward process posteriors, which become manageable when conditioned on  $x_0$ :

$$q(y_{t-1}|y_t, x_0) = \mathcal{N}(y_{t-1}; \tilde{\mu}_t(x_t, x_0), \tilde{\tau}_t I). \quad (6)$$

Where:

$$\tilde{\mu}_t(y_t, y_0) := \left( \frac{\sqrt{\alpha_{t-1}}\beta_t}{(1 - \bar{\alpha}_t)} \right) y_0 + \left( \frac{\sqrt{\alpha_t}(1 - \bar{\alpha}_{t-1})}{(1 - \bar{\alpha}_t)} \right) y_t$$

and

$$\tilde{\tau}_t := \frac{(1 - \bar{\alpha}_{t-1})}{(1 - \bar{\alpha}_t)} \beta_t.$$

As a result, all KL divergences in Equation (5) are comparisons between Gaussian distributions, allowing for their efficient calculation using closed-form expressions [\[3\]](#).

---

**Algorithm 1 - Training a denoising model  $f_\theta$** 

---

- 1: **repeat**
  - 2:  $(\mathbf{x}, \mathbf{y}_0) \sim p(\mathbf{x}, \mathbf{y})$
  - 3:  $\bar{\alpha}_t \sim p(\bar{\alpha}_t)$
  - 4:  $\epsilon \sim \mathcal{N}(\mathbf{0}, \mathbf{I})$
  - 5: Take a gradient descent step on  
$$\nabla_\theta \|f_\theta(\mathbf{x}, \sqrt{\bar{\alpha}_t} \mathbf{y}_0 + \sqrt{1 - \bar{\alpha}_t} \epsilon, \bar{\alpha}_t) - \epsilon\|_p^p$$
  - 6: **until** converged
- 

**Inference via Iterative Refinement**

Our model is defined according to the following iterative algorithm:

---

**Algorithm 2- Inference in  $T$  iterative refinement steps**

---

- 1:  $\mathbf{y}_T \sim \mathcal{N}(\mathbf{0}, \mathbf{I})$
  - 2: **for**  $t = T, \dots, 1$  **do**
  - 3:  $\mathbf{z} \sim \mathcal{N}(\mathbf{0}, \mathbf{I})$  if  $t > 1$ , else  $\mathbf{z} = \mathbf{0}$
  - 4:  $\mathbf{y}_{t-1} = \frac{1}{\sqrt{\alpha_t}} \left( \mathbf{y}_t - \frac{1-\alpha_t}{\sqrt{1-\bar{\alpha}_t}} f_\theta(\mathbf{x}, \mathbf{y}_t, \bar{\alpha}_t) \right) + \sqrt{1 - \alpha_t} \mathbf{z}$
  - 5: **end for**
  - 6: **return**  $\mathbf{y}_0$
- 

This inference process is defined using Gaussian conditional distributions, which provide insight into how the image changes at each step as noise is removed. Furthermore, by using Hugging face class conditioned diffusion model we leverage our denoising model  $f_\theta$  to aid in reversing the diffusion process. This model takes a source image  $\mathbf{x}$  as a condition and a noisy target image  $\tilde{\mathbf{y}}$  including  $\mathbf{y}_t$  as input and attempts to recover the noise-free target image  $\mathbf{y}_0$ .

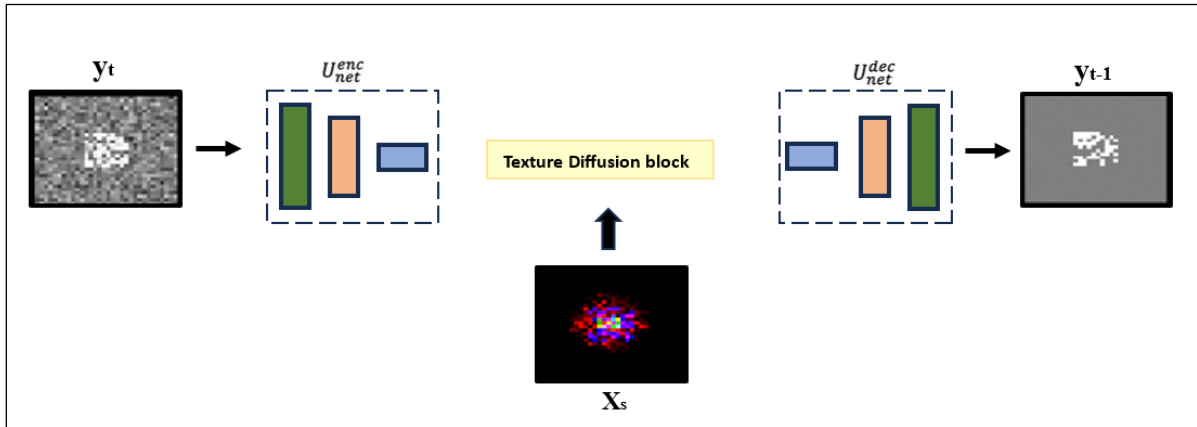


**Figure 7:** The Model Architecture [8]. ( $\mathbf{y}_t$ - noised pattern,  $\mathbf{x}_s$ - light matrix,  $\mathbf{y}_{t-1}$ - denoised pattern)

The reverse process starts from the noisy image  $\mathbf{y}_T$  and gradually denoises it until it reaches the initial image  $\mathbf{y}_0$ . The denoising model  $f_\theta$  is trained to estimate the noise  $\epsilon$  given the noisy image

and the hyperparameters  $\bar{\alpha}_t$  and  $\alpha_t$ . The hyperparameter  $\bar{\alpha}_t$  controls the amount of noise that is removed at each step of the reverse process. A higher value of  $\bar{\alpha}_t$  means that more noise is removed, but it also increases the risk of overfitting. The hyperparameter  $\alpha_t$  controls the variance of the Gaussian conditional distribution  $p_\theta(\mathbf{y}_{t-1} | \mathbf{y}_t, \mathbf{x})$ . A higher value of  $\alpha_t$  means that the distribution is more concentrated around the mean, but it also makes the model more sensitive to the noise in the data. If the noise variance of the forward process steps is set as small as possible, i.e.,  $\alpha_{1:T} \approx 1$ , the optimal reverse process  $p(\mathbf{y}_{t-1} | \mathbf{y}_t, \mathbf{x})$  will be approximately Gaussian. Accordingly, the choice of Gaussian conditionals in the inference process can provide a reasonable fit to the true reverse process. Meanwhile,  $1 - \bar{\alpha}_t$  should be large enough so that  $\mathbf{y}_T$  is approximately distributed according to the prior  $p(\mathbf{y}_T) = \mathcal{N}(\mathbf{y}_T | \mathbf{0}, \mathbf{I})$ , allowing the sampling process to start at pure Gaussian noise. The denoising model  $f_\theta$  is trained to estimate  $\epsilon$ , given any noisy image  $\hat{\mathbf{y}}$  including  $\mathbf{y}_t$ . Thus, given  $\mathbf{y}_t$ , we approximate  $\mathbf{y}_0$  by rearranging the terms in  $\hat{\mathbf{y}}$  (4) as

$$\hat{\mathbf{y}}_0 = \frac{1}{\sqrt{\bar{\alpha}_t}} \left( \mathbf{y}_t - \sqrt{1 - \bar{\alpha}_t} f_\theta(\mathbf{x}, \mathbf{y}_t, \bar{\alpha}_t) \right).$$

We substitute our estimate  $\hat{\mathbf{y}}_0$  into the posterior distribution of  $q(\mathbf{y}_{t-1} | \mathbf{y}_0, \mathbf{y}_t)$  in (6) to parameterize the mean of  $p_\theta(\mathbf{y}_{t-1} | \mathbf{y}_t, \mathbf{x})$  as

$$\mu_\theta(\mathbf{x}, \mathbf{y}_t, \bar{\alpha}_t) = \frac{1}{\sqrt{\alpha_t}} \left( \mathbf{y}_t - \frac{1 - \alpha_t}{\sqrt{1 - \bar{\alpha}_t}} f_\theta(\mathbf{x}, \mathbf{y}_t, \bar{\alpha}_t) \right),$$

and we set the variance of  $p_\theta(\mathbf{y}_{t-1} | \mathbf{y}_t, \mathbf{x})$  to  $(1 - \alpha_t)$ , a default given by the variance of the forward process.

## 4.2 The strengths of our approach

After reviewing the relevant academic papers and literature, we found that the main alternative to our approach is generative adversarial networks (GANs). We assume that our approach is the right thing to do due to the following advantages [\[7\]](#) of diffusion models over GANs:

- **More stable training:** Diffusion models are generally easier to train than GANs. This is because diffusion models do not require an adversarial training process, which can be unstable and difficult to converge.
- **Less prone to mode collapse:** Mode collapse is a problem that can occur in GANs, where the model learns to generate only a small number of output images. Diffusion models are less prone to mode collapse because they do not rely on an adversarial training process.

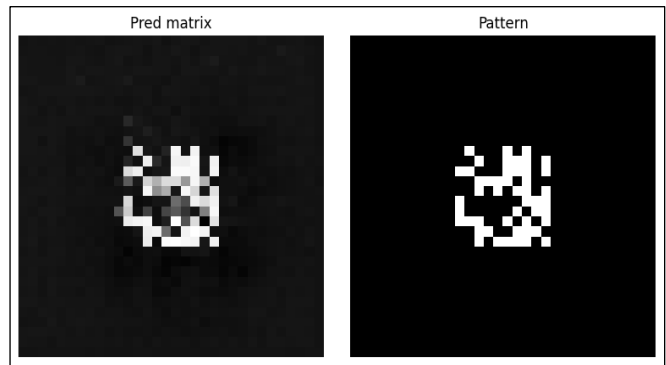


Figure 8: Pattern prediction after 10 epochs

- Better diversity of output images:  
Diffusion models can generate more diverse images than GANs. This is because diffusion models start with a high-entropy latent representation and gradually add noise to it, which allows the model to explore a wider range of possible images.

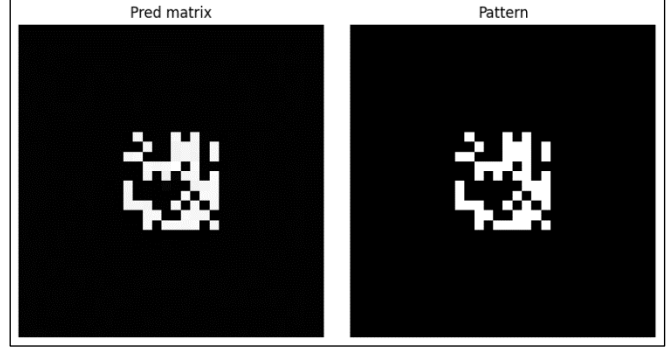


Figure 9: Pattern prediction after 50 epochs

## 5. Experiments

### 5.1 Validation of Problem-Solving Approaches

In our experiments, we chose to use Hugging Face Condition Unet Architecture in order to fit a light matrix to its suitable metasurface pattern. We tried to solve this problem with different approaches and inputs:

1. The Unet model received a  $32 \times 32 \times 1$  pattern as its primary input. Simultaneously, we introduced a  $32 \times 32 \times 3$  light matrix as a conditional input, encompassing transmitted light, reflected light, and the height multiplied by the corresponding pattern.
2. Similarly, the Unet model took a  $32 \times 32 \times 1$  pattern as input, with a  $32 \times 32 \times 3$  light matrix as a conditional input. The light matrix included transmitted light, reflected light, and a constant height value.
3. In an alternative approach, we fed a  $32 \times 32 \times 4$  pattern concatenated with a light matrix into the Unet model. Additionally, the metasurface height served as the conditional input.

After a thorough evaluation, we settled on the first approach. The second approach was less accurate after 50 epochs compared to the first, and the third approach failed to converge altogether.

### 5.2 Results Visualization

To enhance the clarity of our experimental findings, we have incorporated graphs, tables, and visualizations throughout the following sections. These visual aids are intended to offer a comprehensive understanding of the model's performance. Our initial analysis executed the model with varying batch sizes of 16, 20, 24, and 32 across 50 epochs.

batch size	16			20			24			32		
Loss Function	MSELoss()	L1Loss()	HuberLoss()	MSELoss()	L1Loss()	HuberLoss()	MSELoss()	L1Loss()	HuberLoss()	MSELoss()	L1Loss()	HuberLoss()
Learning Rate												
1.0e-02	0.046664	0.053940	0.023332	0.047459	0.051601	0.023732	0.046662	0.050402	0.023332	0.484380	0.052113	0.024217
2.0e-01	0.047020	0.113538	0.023508	0.047689	0.062936	0.023836	0.252047	0.089244	0.023331	0.048520	0.232394	0.024259
3.0e-04	0.000005	0.000303	0.000002	0.000006	0.000705	0.000003	0.000011	0.000463	0.000007	0.000005	0.000549	0.000002
4.0e-03	0.000036	0.031949	0.000028	0.000060	0.005799	0.000013	0.000074	0.036567	0.000027	0.000181	0.028004	0.000063

Table 2: learning rate loss function for each batch



Each run of the model corresponding to one of the batch sizes, encompassed the application of three distinct loss functions: MSELoss, L1 Loss, and HuberLoss. by the following table, we can notice that the best accuracy is found under the HuberLoss column with leaning rate  $3e^{-04}$  and batch 20.

However, after testing the model we discovered that the prediction is less accurate in comparison to the MSELoss with the same parameters even though the loss in the training model is lower by using the Huber Loss. We assume it happened due to the overfitting of the training model. By the following graph, we notice that the optimal batch for our model is batch 20 because it contains the lowest loss over each one of the loss functions Although there is no

directly comparable classification project for benchmarking our results, we can make an observation by examining the performance of the same model architecture on an image restoration problem on the Hugging Face website. We find that the loss curve of the model for the classifying problem is similar to the loss curve of the same model used for image restoration on the Hugging Face website.

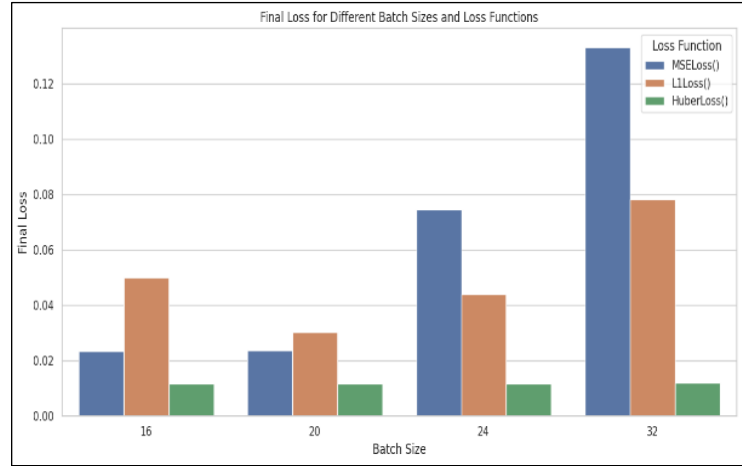


**Figure 10:** Final loss for different batch sizes and loss functions graph

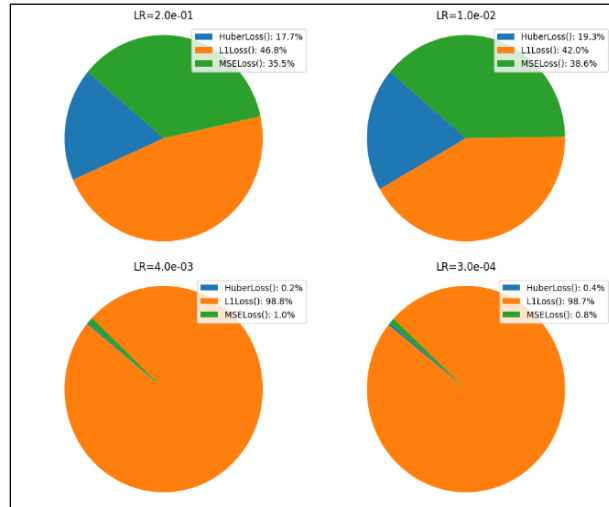


**Figure 11:** A graph of different loss functions and learning rate for batch 20

### 5.3 Addressing Failure Modes in Our Model

- **Overfitting:** By using the Huber Loss function during the training of the model, we obtained the lowest loss values with a required predicted pattern. However, after testing the model, the predicted pattern was relatively blurred in comparison to the MSE Loss function. We assume that the reason for the blurred output is due to overfitting which is a common problem in machine learning and statistical modeling that occurs when a model learns the training data too well.

- **Excessive Layering:** Experimenting with a 128-layer model led to a surprising outcome – a blank output resembling a white square with no discernible structure to the target pattern.
- **Inadequate Data Preparation:** When we inserted the input data into the model, we observed that the height values were too high relative to the transmitted light, and reflected light values thus the representation of them in the light matrix was barely

noticeable and had negligible influence in the training model. We solved this problem by normalizing each one of the parameters.

- High Learning Rate: Opting for a large learning rate resulted in a notable spike in the loss curve during training, particularly evident in the 6th epoch. To address this, we reduced the learning rate to  $3e^{-04}$ , yielding a more consistent and gradual decrease in the loss curve, as depicted in the subsequent figure.

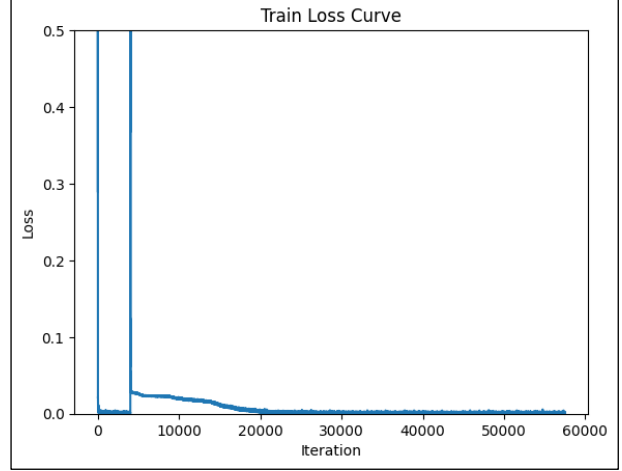


**Figure 12:** The training loss graph (batch =20, lr=  $4e^{-3}$ , MSELoss)

## 6. Conclusions

Through experimentation, we determined that setting the parameters as follows - a learning rate of  $3e^{-04}$ , a batch size of 20, and employing the Mean Squared Error (MSE) Loss function. The model yielded accurate predictions of the required metasurface pattern after approximately 50 training epochs.

### 6.1 Observations

After the training and testing of our diffusion model, we learned the following:

Leveraging Pre-built Models: Throughout the project, we transitioned from the practice of constructing models from the ground up to utilizing pre-existing models from Hugging Face. This shift in approach allowed us to streamline our development process and leverage state-of-the-art resources effectively.

Conditional Input in Diffusion Models: An intriguing aspect of our project involved utilizing a conditional input, represented by the light matrix in our case, to classify the noisy input of the metasurface. This approach was new to us as, traditionally, diffusion models are primarily associated with tasks like segmentation, restoration, and high-definition image generation, rather than fitting and classification tasks. This experience expanded our understanding of the versatility of diffusion models and their applicability in diverse problem domains.

### 6.2 Ideas for future extensions or new applications

- In this project we used the Google Colab and cloud service to process the diffusion model. A possible future extension can be deploying the model on hardware accelerators to ensure fast and efficient predictions.
- Interactive User Interface:

Develop an interactive user interface such as a smartphone application that allows users to input different parameters and visualize the predicted metasurface patterns in real time.

- Fine-tune the model parameters to achieve even greater optimization and identify a more efficient optimizer, aiming to accelerate the training process significantly and improving the accuracy of the metasurface pattern prediction.
- Multi-Modal Learning:  
Explore the integration of multiple modalities into the diffusion model. For example, incorporate additional types of data such as thermal or infrared imaging to enhance the model's ability to predict metasurface patterns under various conditions.

## 7. Appendix

- [1] Hugging Face Diffusion Models Course: <https://github.com/huggingface/diffusion-models-class/tree/main>
- [2] Mahmoud M. R. Elsawy, Stéphane Lanteri, Régis Duvigneau, Jonathan A. Fan, and Patrice Genevet. **Numerical Optimization Methods for Metasurfaces: Laser Photonics**, Rev. 2020, 14, 1900445.
- [3] Chitwan Saharia<sup>†</sup>, Jonathan Ho, William Chan, Tim Salimans, David J. Fleet, Mohammad Norouzi. **Image Super-Resolution via Iterative Refinement**, arXiv:2104.07636v2 30 Jun 2021.
- [4] Florinel-Alin Croitoru, Vlad Hondru, Radu Tudor Ionescu, and Mubarak Shah. **Diffusion Models in Vision: A Survey**, arXiv:2209.04747v2 6 Oct 2022.
- [5] Jonathan Ho, Ajay Jain, Pieter Abbeel. **Denoising Diffusion Probabilistic Models**, arXiv:2104.07636v2 30 Jun 2021.
- [6] Ling Yang Zhilong Zhang, Yang Song, Shenda Hong, Runsheng Xu, Yue Zhao, Wentao Zhang, Bin Cui, Ming-Hsuan Yang. **Diffusion Models: A Comprehensive Survey of Methods and Applications**, arXiv:2209.00796v10 23 Mar 2023.
- [7] Prafulla Dhariwal and Alex Nichol. **Diffusion Models Beat GANs on Image Synthesis**, arXiv:2105.05233v4 1 Jun 2021.
- [8] Ankan Kumar Bhunia, Salman Khan, Hisham Cholakkal, Rao Muhammad Anwer, Jorma Laaksonen, Mubarak Shah, Fahad Shahbaz Khan, Mohamed bin Zayed. **Person Image Synthesis via Denoising Diffusion Model**, arXiv:2211.12500v2 28 Feb 2023.
- [9] Our code: [https://github.com/Nadavmarci/DeepLearning\\_Course\\_TAU/blob/main/FinalProject.ipynb](https://github.com/Nadavmarci/DeepLearning_Course_TAU/blob/main/FinalProject.ipynb)